THE JOURNAL OF PHYSICAL CHEMISTRY C

pubs.acs.org/JPCC Article

Plasmonic Electricity II: The Effect of Particle Size, Solvent Permittivity, Applied Voltage, and Temperature on Fluorophore-Induced Plasmonic Current

Joshua Moskowitz, Rashad Sindi, and Chris D. Geddes*

Cite This: J. Phys. Chem. C 2020, 124, 5780−5788 Read Online

ACCESS | Metrics & More | Article Recommendations | Supporting Information

ABSTRACT: In a recent paper, our laboratory has shown that fluorophores in close proximity to a non-continuous metal nanoparticle film can induce a detectable electrical current in the film. This current was found directly proportional to the fluorophore extinction coefficient and concentration when excited with p-polarized light. This finding threatens to change the way we both think about and use fluorescence spectroscopy as no longer do we have to use and are limited by traditional photodetectors and associated optics to collect and measure fluorescence signatures. This approach holds potential to significantly simplify fluorescence-based instrumentation. In this paper, we significantly expand upon our previous findings and show that plasmonic current is a function of the nanoparticle size and spacing in the film, which is explained by the concentric sphere model for nanoparticle capacitance. We also demonstrate the dependence of plasmonic current on the relative permittivity of the solvent, and that in an excess of salt, the fluorophore-induced current is significantly greater than the background current. This paves the way for downstream plasmonic assays in a variety of biological media. In addition, we have measured plasmonic current as a function of both applied bias voltage and temperature, allowing for the optimization of the fluorophore-induced plasmonic current. These findings allow for not only a better understanding of plasmonic current but also its optimization as it relates to fluorescence-based detection.

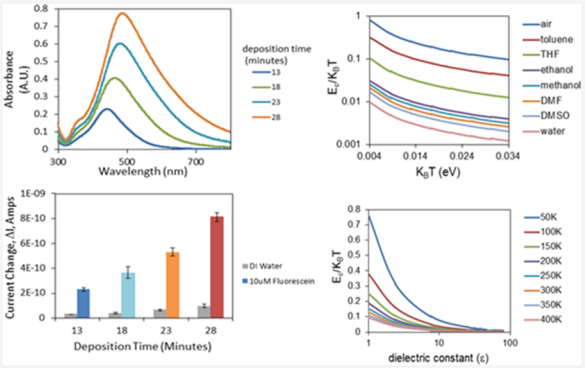

INTRODUCTION

Recent advances in both nanoscience and in the understanding of plasmonics have led to a rise in the number of "plasmon to current" technologies being introduced in the literature. These technologies allow for the electrical detection of plasmon resonance and often function via energy transfer from a dephasing plasmon to a semiconductor, generating an electrical current in the semiconductor.[1−5] While these devices have demonstrated promise in solar cells, their applicability in molecular detection is very limited as "plasmon to light" techniques, such as surface plasmon resonance, are often employed for detection purposes.[6−10]

In a recent paper, our laboratory has described a "plasmon to current" technique that functions via electron transport or "hopping" between separate metal nanoparticle islands, generating a measurable electrical current.[11] This current is found to increase upon excitation of a proximal fluorescent molecule and is found to be dependent on the fluorophore extinction coefficient.[11] This observation is explained by non-radiative energy transfer from the molecule to the metal particle and the subsequent plasmon relaxation via electron transport between the metal nanoparticle islands (Figure 1). An increased fluorophore extinction coefficient is expected to

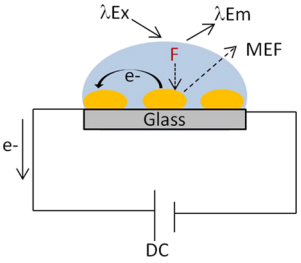

Figure 1. Schematic depicting non-radiative energy transfer from a fluorophore (F) to metal nanoparticle islands and subsequent electron transport between particles. The blue color represents a liquid solvent. Electrodes are in simultaneous contact with the metal film and solvent.[11]

Received: December 4, 2019
Revised: February 10, 2020
Published: February 18, 2020

facilitate an increase in energy in the near-electric field of the nanoparticle, ultimately resulting in more energy transfer from the fluorophore to the metal particle. The strength of direct coupling between far-field radiation (excitation light) and the metal nanoparticles decreases as the particles grow toward the wavelength of incoming light.[5] Metal particles in our films are relatively large (~50 nm), displaying broadened extinction spectrums, and only weakly coupling with far-field light. However, these particles may still couple strongly with local near-field fluorophores, exciting plasmon resonances, and subsequently generating electrical current directly in the metal nanoparticle film.[11,12]

Electrical DC current in the plasmonic current technique is dependent on a number of factors, including particle size and spacing in the film, solvent permittivity, applied voltage, and temperature. Understanding how these parameters effect plasmonic current is critical to the optimization of the plasmonic current technique to a variety of fluorescence-based applications including in molecular detection assays, where inconsistencies in these parameters could well represent a limitation to the development of robust detection assays.

The dependence of the induced electrical current on the particle size and relative permittivity of the medium between nanoparticles is described by the simple sphere model for capacitance of a single nanoparticle, that is

$$C = 2\pi\varepsilon_0\varepsilon d \tag{1}$$

where ε_0 is the vacuum permittivity, ε is the static relative permittivity of the medium surrounding the particle, and d is the diameter of a spherical particle.[11,13,14] As particles in our films are completely surrounded by neighboring particles, the concentric sphere model may be used to calculate the capacitance, which is a common approach throughout the literature.[14−18] This model also includes the permittivity of the medium between particles:

$$C = 4\pi\varepsilon_0\varepsilon r_0(r_0 + s)/s \tag{2}$$

where r_0 is the particle radius, and s is the distance between two neighboring particles. In a previous paper, our laboratory has expanded this model to include the capacitance between two distant points in the nanoparticle island film.[11] The capacitance is then related to the charging energy required for a nanoparticle to gain an electron by

$$E_c = \frac{e^2}{2C} \tag{3}$$

where E_c is the charging energy, e is the elementary electric charge, and C is the capacitance of the particle.[13,14,19,20] Therefore, increased nanoparticle size and decreased spacing between nanoparticles in the film and an increased permittivity of the solvent between the nanoparticles would be expected to lead to a higher nanoparticle capacitance. This increased capacitance then leads to a lower charging energy required for the particle to gain an electron (eq 3). In other words, electron transport between metal particles is favored when the particles are relatively large and closely spaced, and the metal films are immersed with high permittivity solvents. This increase in permittivity is expected to increase both the dark current (background signal) and the much greater magnitude fluorophore-induced electrical current,[11] with potential for optimization of the device signal-to-noise ratio through manipulation of the solvent permittivity. In addition, the ability of the plasmonic current technique to generate a fluorophore-induced current in media with a variety of permittivity values opens the possibility for molecular detection assays conducted directly in biological/chemical matrices.

In addition to particle size and solvent permittivity, the thermal energy of the system can also be expected to affect the fluorophore-induced plasmonic current. Under a zero voltage applied external bias, electron transport between separate metal nanoparticles occurs when the thermal energy of the system is greater than the charging energy:[13,14,19,20]

$$E_c < k_B T \tag{4}$$

where k_B is the Boltzmann constant. It is therefore expected that increased temperatures will lead to thermally activated electron transport through the metal nanoparticle island film. The ratio of $E_c/k_B T$ may then provide a measure of electron transport in the nanoparticle film under study, where ratios below 1 are expected to result in electron transport and a measurable current under zero applied bias. We subsequently questioned the role of temperature on the fluorophore-induced current, with the aim of determining the optimal temperature for fluorophore-induced current generation.

In addition to temperature, an applied external bias voltage across the nanoparticle films is also expected to influence the fluorophore-induced electrical signal. This applied voltage has several potential advantages over zero applied voltage (although every current measuring instrument does provide some inherent bias itself). One such advantage that we have observed is in the stabilization of the background current (i.e., no fluorophore), which can otherwise display fluctuations due to inhomogeneity in the nanoparticle island film surface. The background current stabilization then allows for a much higher signal-to-noise ratio upon excitation of a suitable proximal fluorophore. Further, an applied bias allows for control over directionality in the film (in essence circuit), leading to more consistent and reproducible measurements. Finally, an external applied voltage is expected to help overcome the Coulombic blockade to electron transport between discreet metal nanoparticles, lowering the energy requirement from the fluorophore for the induced signal. However, at relatively large bias voltages (>0.1 volts) production of a large current provides increased background noise, preventing a detectable signal upon fluorophore excitation. In addition, the use of a relatively large current is expected to alter the fluorophore, preventing the relaxation of electrons in the fluorophore and ultimately energy transfer to the metal nanoparticles. We have subsequently investigated the induced current over a wide range of applied voltages in order to optimize the signal response from the fluorophore and to better understand the fluorophore-induced plasmonic current process.

In this paper, we subsequently report the dependence of the fluorophore-induced current on several key factors including particle size and spacing, solvent permittivity, temperature, and applied bias voltage. In addition, we characterize electron transport in our metal nanoparticle island films in terms of these variables, increasing our understanding of the fluorophore-induced electrical signal. Finally, we place these findings in context in terms of the downstream optimization of these parameters for future informative molecular detection assays with increased sensitivity.

https://dx.doi.org/10.1021/acs.jpcc.9b11276
J. Phys. Chem. C 2020, 124, 5780−5788

RESULTS AND DISCUSSION

Dependence of Induced Current on Nanoparticle Size and Spacing. It was speculated that as surface nanoparticles grow larger and more closely spaced, upon fluorophore excitation, increased electron transport will lead to an observed electrical current increase. This may be explained by a decreased particle charging energy and lower Coulombic gap to electron "hopping" in the larger and more closely spaced particles. In order to demonstrate the effect of varying particle size and spacing on plasmonic current generation, films were subsequently prepared at various thermal vapor deposition times, leading to a range of particle size and spaces. Scanning electron microscopy (SEM) images with particle size analysis are shown in Figure 2a. A comparison of Figures 2a and 2b

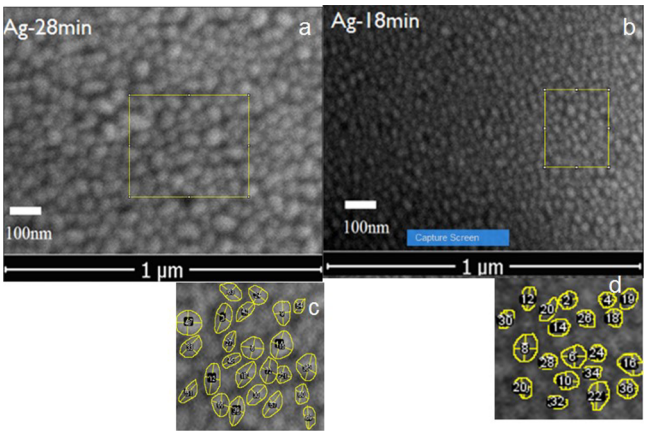

Figure 2. Silver films produced at (a, c) 28 min and (b, d) 18 min thermal vapor deposition times. The deposition rate was held constant at 0.1 Å/s. (c, d) Particle size analysis conducted with ImageJ software. The regions of interest in panels (a) and (b) are enlarged for analysis in panels (c) and (d), respectively.

demonstrates the increase in the average particle size in the film in going from a 18 to 28 min thermal vapor deposition time. As the particles grow toward each other in the film, the spacing between particles subsequently decreases. Particle size distributions along with a table of average particle and nearest-neighbor spacing distances are shown in Supplemental Figure S1 and Table S1, respectively. Figure S1 shows particles produced with the 18 min thermal vapor deposition time to be relatively spherical compared to higher deposition times, with a diameter of ∼28 nm and an aspect ratio of ∼1.2. As the deposition time is increased to 28 min, the particles become larger and more elliptical, with a length of ∼57 nm and an aspect ratio of ∼1.5. The overall particle area is found to increase from 641 to 1687 nm^2 for the 18 and 28 min deposition times, respectively. Figure 3a contains UV−Vis absorption spectra of silver films produced over a range of thermal vapor deposition times, demonstrating control over the optical properties of the films. An observed red-shifted and broadened absorption spectrum in Figure 3a is indicative of the growing of the average particle size in the film.[5] It is expected that, as these sizes grow, the spacing between particles decreases, and this is supported by a transformation from non-continuous (zero measurable current) to low resistance continuous metal films (1 Ω). In other words, the particles grow into each other, decreasing the size of spaces between the particles.

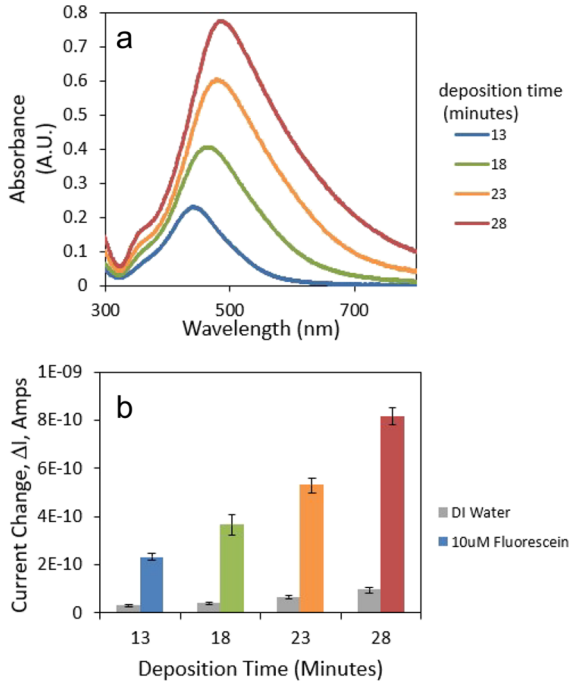

Figure 3. (a) Absorption spectra of silver island films produced over a range of thermal vapor deposition times. (b) Observed current change upon 473 nm excitation of a 10 μM aqueous fluorescein solution coated on the silver nanoparticle films.

Figure 3b shows the induced current, upon fluorophore excitation, as a function of film synthesis thermal vapor deposition time. Figure 3b also correlates these measurements with the film absorption spectra in Figure 3a. Results demonstrate a clear upward trend in current change as a function of film deposition time in both silver and gold films (Supplemental Figure S2). This trend may be explained by an increased potential for electron transport with fluorophore excitation in the films produced at higher deposition times. This is because these longer deposition times lead to larger and more closely spaced particles, that is, eq 2 above, leading to a greater capacitance and lower charging energy required for electron transport in the film.

Effect of Solvent Permittivity on Fluorophore-Induced Current. In order to investigate the dependence of the background plasmonic current on solvent permittivity, various solvents were coated onto silver and gold nanoparticle island films. The solvents were chosen in order to provide a range of permittivity values (ε), which is expected to influence the electron transport rate across the film according to eq 2 above. Figure 4 shows the current generation over the range of solvents. An upward trend is observed, demonstrating that an increased solvent permittivity results in an increased current generation. This is explained by the fact that electrons may "hop" between separate metal particles more easily through a medium of higher permittivity (eq 2).

We have subsequently undertaken simulations to demonstrate the effect of solvent permittivity on the ratio of E_c/k_BT at various temperatures (Figure 5). Here, E_c is determined with the concentric sphere model described above, and k_BT is the thermal energy of the system. As the solvent dielectric constant increases, E_c/k_BT decreases, providing for increased electron transport. This lowers the energy requirement from the fluorophore for current induction, which ultimately leads to

https://dx.doi.org/10.1021/acs.jpcc.9b11276
J. Phys. Chem. C 2020, 124, 5780−5788

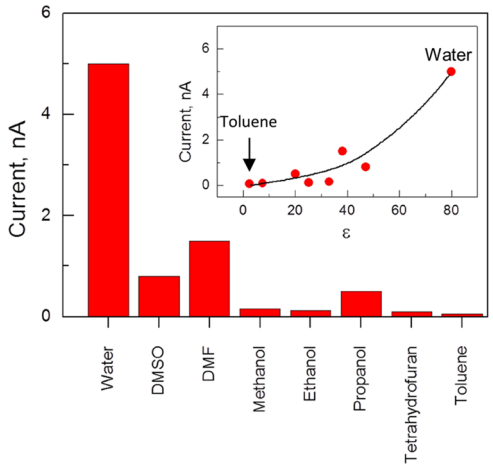

Figure 4. Induced current from silver island films (SiFs) from various solvents. (Inset) Induced current as a function of solvent dielectric constant, that is, (relative permittivity), ε.

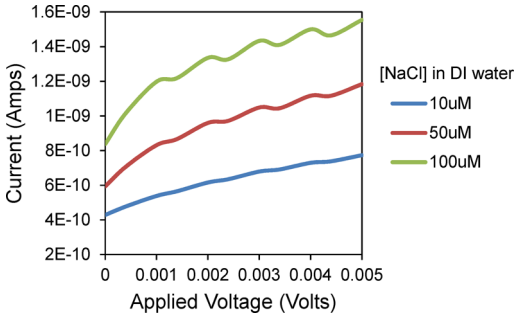

Figure 6. $I-V$ curves for a DI water solvent covered gold island film over a range of NaCl concentrations.

a greater observed electrical signal upon fluorophore excitation. Figure 5b shows the importance of temperature on the relationship between solvent dielectric constant and E_c/k_BT. Here, as temperature decreases, E_c/k_BT becomes significantly larger at low dielectric constants. This is because, at low dielectric constants, decreasing the temperature strongly prevents electron transport through the film.

To understand electron hopping between nanoparticles further, we have measured the current (I) versus voltage (V) curves. Figure 6 shows $I-V$ curves for an aqueous solvent covered silver island film over a range of NaCl concentrations. The curves are non-ohmic and display a Coulombic staircase, as we have shown in a previous paper.[11] This observation is due to the ability of an increased voltage to overcome the Coulombic blockade, allowing for electron transport across the film. Here, an increased current and increased slope in the $I-V$ curve is observed with increasing salt concentration. This is due to the increased solvent permittivity in eq 2, leading to a higher nanoparticle capacitance. This decreases the charging energy of the particle, leading to increased electron "hopping" between the discreet silver islands and a subsequent increase in the observed current.

Similarly, we have investigated the fluorophore-induced current in solutions of varying salt content. Figure 7 shows the induced signal as function of both solvent conductivity and NaCl concentration. Here, it is expected that an increased salt concentration leads to a greater permittivity in eq 2, increasing electron transport and the observed electrical current. Figure 7a demonstrates a large increase in the fluorophore-induced signal with increasing solution conductivity. From Figure 7b, it is clear that excitation of the fluorophore in an excess of salt leads to a large measurable fluorophore signal. Building on this concept, Figure 8 shows the background current in various matrices. Moving from left to right in Figure 8, it can be seen that, as the salt content of the medium is increased, the background current also increases. However, looking at the final bar in Figure 8, we can see that excitation of the fluorophore in an excess of salt (~50 mM salt in a urine matrix[21]) leads to a large spike in the electrical current, which is due to the presence of the fluorophore. This is useful as it opens up the potential for the construction of plasmonic current assays directly in various biological and environmental mediums, that is, the induced plasmonic current is much greater than the background current from an increase in either salt concentration or solution permittivity.

Effect of Voltage Bias on Fluorophore-Induced Plasmonic Current. The application of a bias voltage to metal nanoparticle films holds potential for both the control over directionality in the circuit and lowering the energy requirement of the fluorophore for electrical current generation. For example, if the charging energy required for electron transport is relatively large with zero applied bias, in this case, the excitation of the fluorophore may not provide enough energy to overcome the Coulombic blockade and induce a current change. However, the application of a small voltage may subsequently help to overcome the blockade, providing for increased current generation upon fluorophore excitation. Conversely, if a relatively high voltage is applied, the background current through the system may now be too high for a detectable current change with excitation of the proximal fluorophore. In other words, the electrical signal generated from the fluorophore should aim to rise above the background

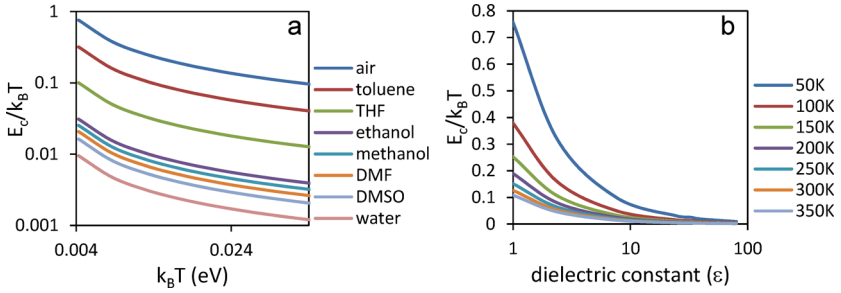

Figure 5. Simulations showing (a) ratio of charging energy to thermal energy (E_c/k_BT) decreases with increasing solvent dielectric constant. (b) At a lower dielectric constant, E_c/k_BT varies more with temperature.

https://dx.doi.org/10.1021/acs.jpcc.9b11276
J. Phys. Chem. C 2020, 124, 5780−5788

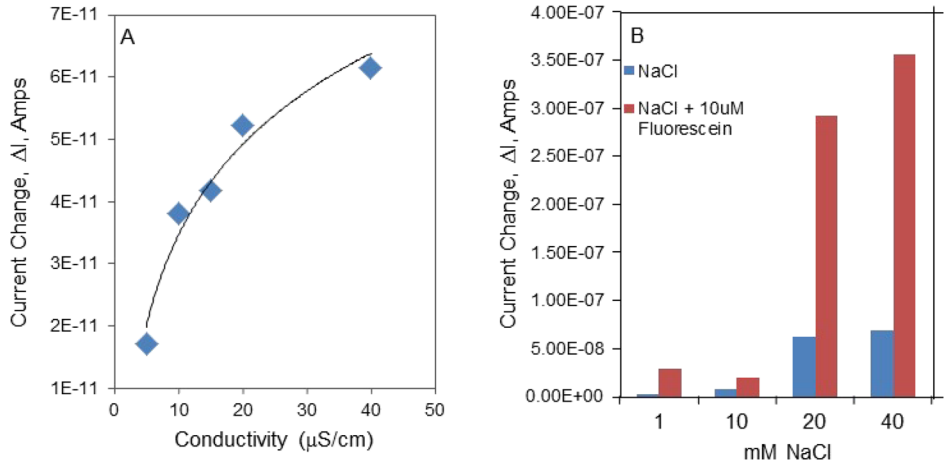

Figure 7. (A) Dependence of fluorophore-induced plasmonic current from a silver island film (SiF) upon its solvent conductivity in aqueous solution. Current in the system was induced with 532 nm laser excitation of rhodamine b. (B) Current resulting from NaCl and NaCl plus 10 μM fluorescein on a silver island film.

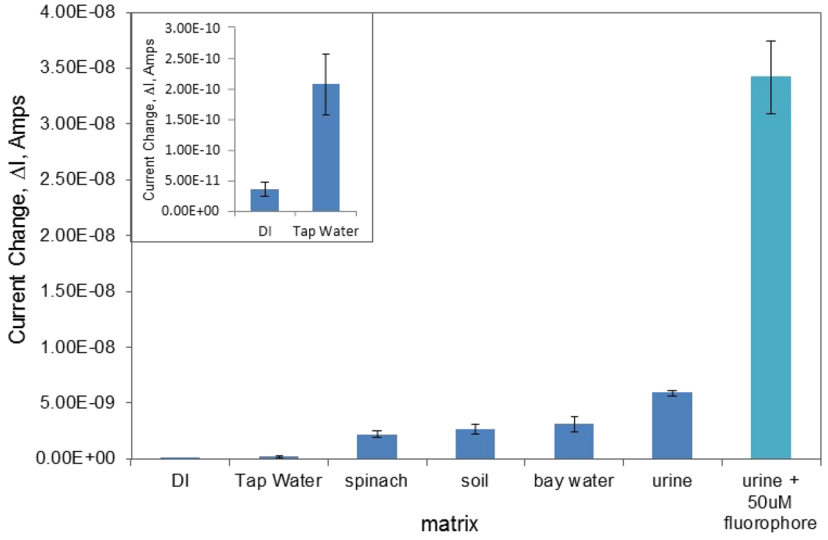

Figure 8. Background electrical current from various aqueous solution matrices on a silver island film. The fluorophore used was fluorescein and was excited at 473 nm. Error bars represent the mean of three measurements.

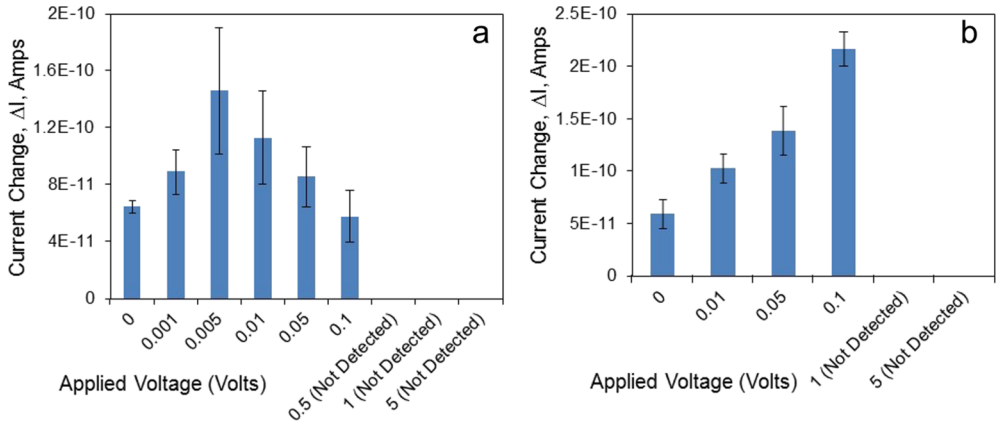

Figure 9. Fluorophore-induced current as a function of applied voltage. (a) 10 μM aqueous sulforhodamine 101 excited with a 594 nm light-emitting diode (LED) on a gold island film. (b) 10 μM aqueous fluorescein excited with a 473 nm LED on a silver island film.

current as much as possible, which may be difficult with a high background induced by a relatively large voltage. We have subsequently studied this dichotomy and measured the fluorophore-induced current over a range of voltages with the goal of optimizing the induced electrical signal. Figure 9 shows the fluorophore-induced current change as a function of

https://dx.doi.org/10.1021/acs.jpcc.9b11276
J. Phys. Chem. C 2020, 124, 5780−5788

applied voltage. Looking at the gold film (Figure 9a), it can be seen that an applied bias of 0.005 volts leads to the greatest signal change. Above an applied voltage of 0.1 volts, the signal change with fluorophore excitation was found to be below the minimum distinguishable signal, which was taken as the sum of the mean solvent blank signal plus three times the standard deviation of multiple solvent blank measurements and calculated to be 4.93×10^{-11} Amps. These values were then reported as not detected. Applied voltages of 0.005 and 0.5 volts were found to produce percent signal differences with fluorophore excitation of >200 and <1%, respectively. This finding is significant as it describes the importance of a relatively small voltage in the induced electrical signal. A similar trend was observed in a silver island film (Figure 9b), with the optimum voltage at 0.1 volts, followed by a decrease in fluorophore-induced signal at higher applied voltages. This data demonstrates that a relatively small voltage may be applied in order to increase electron transport in the system, providing for an increased observed signal upon subsequent fluorophore excitation. However, at relatively large bias voltages, the high background current hinders observation of the fluorophore-induced signal.

Dependence of the Fluorophore-Induced Current on Temperature. In addition to an applied bias, the thermal energy of the system is also expected to influence electron transport and the fluorophore-induced current. A comparison of the metal particle charging energy and the thermal energy provides an informative measure of electron transport in the system. Figure 5 shows the ratio of charging energy to thermal energy for various mediums. Here, the charging energy is estimated with the concentric sphere model described earlier. The ratio of E_c/k_BT measures the potential for electron transport in the system, where a higher ratio indicates less current flow through the metal nanoparticles. Figure 10a shows the magnitude of electrical current through a dry gold island film as a function of temperature with no fluorophore present. The current is found to increase as a function of temperature, suggesting a thermally activated process. In other words, at increased temperatures, a larger population of nanoparticles will be capable of electron transport. Applying the Boltzmann distribution[22]

$$I \propto \frac{N_i}{N} = \frac{e^{-E_c/kt}}{\sum e^{-E_j/kt}} \quad (5)$$

where I is the measured current, and N_i and N are the number of particles that gain an electron and the total particles in the system, respectively. E_j is the energy of either the charged or uncharged state in the two-state system. E_c is taken as the energy required to move an electron across the film between the two electrodes. E_c is calculated from substitution of the concentric sphere model into the grid model for a large number of identical capacitors, which is described in detail in a recent paper from our laboratory.[11] The total number of particles between the electrodes in the film, N, is estimated from SEM images in Figure 2 and film dimensions to be $\approx 1.8 \times 10^{10}$ particles. In this calculation, a spherical particle diameter estimate of 40 nm with a 2 nm gap between adjacent particles is used, along with a 1 cm nanoparticle film length and a 3.2 mm electrode width. This leads to a value of N_i for a gold nanoparticle island film in air at room temperature of 1.6×10^9 particles. This value corresponds to a relatively small percentage, ~9%, of particles in the film with sufficient energy

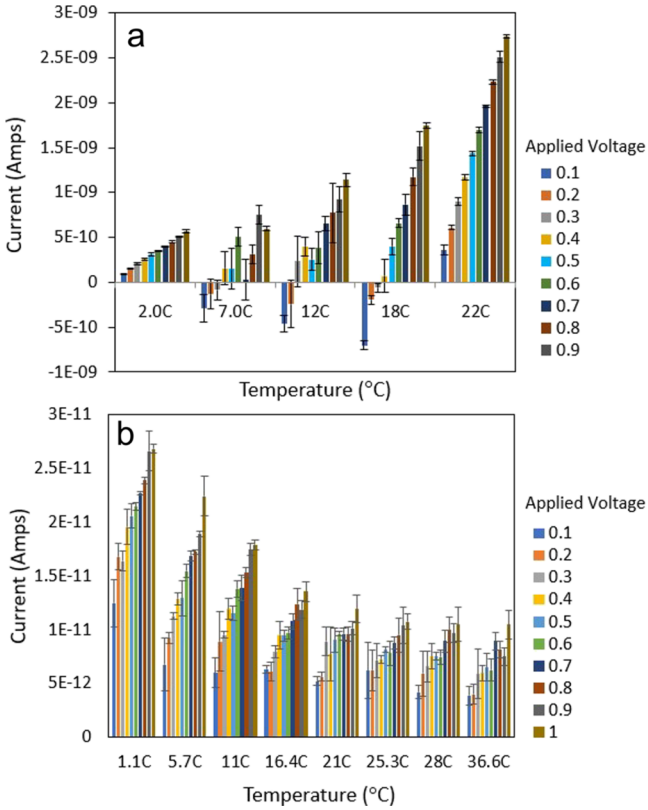

Figure 10. Electrical current as a function of temperature through (a) a dry gold island film and (b) a dry silver island film over a range of applied voltages. Error bars are the mean current from three separate measurements.

for electron transport. This is consistent with our experimental observation of zero measurable electrical current through the dry film at room temperature under a zero applied bias. However, as the permittivity of the medium surrounding the particles, temperature, and applied bias increase, E_c decreases, raising N_i and increasing the measureable electrical current. A comparison of the $I-V$ slopes at various temperatures within Figure 10a demonstrate an increased slope at elevated temperatures. For example, slopes at 2 and 22 °C were calculated to be 4.8×10^{-10} and 2.4×10^{-9} amps/volt, respectively. This increase is due to the increased electron transport through the film with increasing temperature for a given voltage. In other words, when the thermal energy of the system is increased, electrons have an increased ability for "hopping" in the presence of an applied voltage. Further, examination of Figure 10a at the lowest voltages of 0.1 volts over several temperatures demonstrates a lack of directionality in the current flow at this lowest voltage, with an observed negative current over several temperatures. This negative current at a low voltage of 0.1 volts is due to the voltage providing insufficient energy to control (or bias) the directionality of the electron flow. This subsequently allows the temperature to become the more dominant factor at this low voltage, leading to a loss of directionality and a negative observed current.

Figure 10b shows the temperature dependence of current through a dry silver island film. At relatively low temperatures and high applied bias, the island film is found to display properties of the bulk metal, with an inverse relationship between the current and temperature. This observation

https://dx.doi.org/10.1021/acs.jpcc.9b11276
J. Phys. Chem. C 2020, 124, 5780−5788

provides information regarding the electron transport mechanism in the film and is indicative of a quantum mechanical tunneling process in the dry silver film at relatively low temperatures.[23] The thermally activated process in the dry gold film may be due to either quantum mechanical tunneling between adjacent particles or thermionic emission in which electrons leave a metal particle and arrive at another distant particle in the film.[23] Application of an aqueous solvent coating to the metal films is expected to alter the current−temperature relationship and favor electron "hopping" over quantum mechanical tunneling due to the increased permittivity of the solvent, and a thermally activated process was observed for both gold and silver solvent coated films.

Experimental $I-V$ curves for an aqueous fluorophore coated silver island film over a range of temperatures are shown in Figure 11. These curves are non-ohmic and display evidence

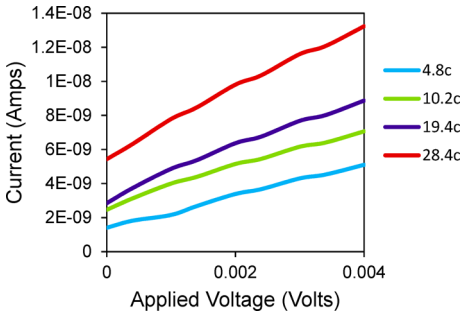

Figure 11. $I-V$ curves for a 10 μM aqueous fluorescein solution coated silver island film over a range of temperatures.

for a Coulombic staircase, which implies that an increased voltage is needed to overcome the Coulombic blockade, allowing for increased electron "hopping" through the film. Here, increasing the temperature is found to provide for both a greater current and greater slope in the $I-V$ curve. These two observations are due to increased thermally activated electron transport through the film under the same applied voltage bias.

The induced current change upon fluorophore excitation as a function of temperature in gold and silver island films is shown in Figure 12. An upward trend is observed, indicating a thermally activated process. A higher temperature provides increased thermal energy, which helps to overcome the Coulombic blockade and provide for increased electron transport through the system. Excitation of the fluorophore is then found to result in a greater measurable signal at increased temperatures. At very low temperatures, electron transport is hindered, and excitation of the fluorophore does not provide sufficient energy for a significant current increase. These results demonstrate that control over both the voltage and temperature may be used to increase the electrical signal with excitation of the fluorophore, opening up the possibility for both control and optimization of the fluorophore-induced current.

CONCLUSIONS

In summary, we have investigated the dependence of fluorophore-induced plasmonic current on several factors including nanoparticle size and spacing, solvent permittivity, applied voltage, and temperature. We have found relatively large and closely spaced particles to result in increased fluorophore-induced current. This is explained through an increase in particle capacitance, leading to an increase in electron transport across the film. In addition, we have found an increase in solvent permittivity to provide for increased electron transport in metal nanoparticle island films and a subsequent increase in the fluorophore-induced electrical signal. This is explained through modeling of the film capacitance, which includes the solvent dielectric constant, and is related to the charging energy of nanoparticles in the film. In this paper, we have also demonstrated the generation of fluorophore-induced current in media containing an excess of salt. This is significant as it opens up the possibility for plasmonic current assays directly in a variety of biological media, such as urine or whole blood. Fluorophore signal optimization has been achieved through the application of a small bias voltage. This is possible because the small voltage helps to overcome the Coulombic blockade, allowing for increased electron transport through the metal island film. However, we have also found conversely that a relatively high applied voltage increases the background noise, preventing a measurable fluorophore-induced electrical signal. We have measured the dependence of the induced signal on the thermal energy of the system. In an analogous manner to an applied

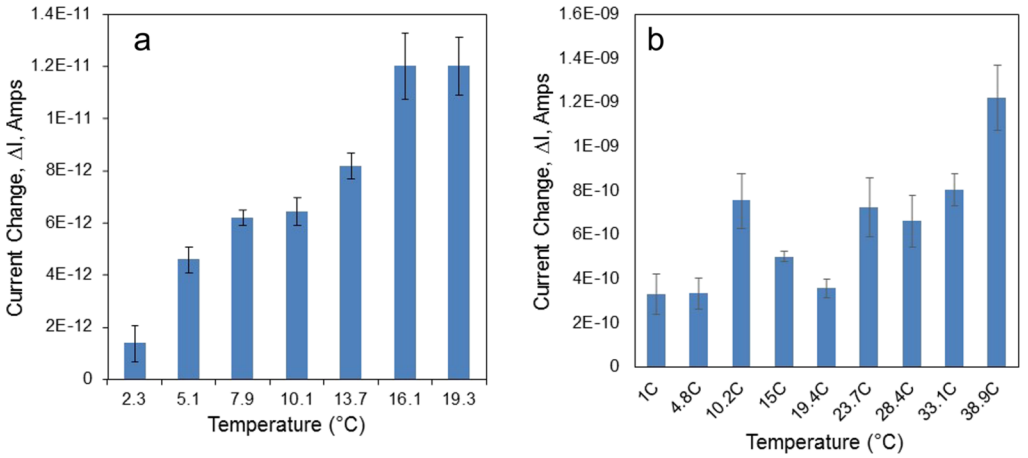

Figure 12. Change in electrical current upon fluorophore excitation as a function of temperature. (a) 20 μM aqueous sulforhodamine 101 on a gold island film with 574 nm LED excitation and a 0.5 millivolt applied bias. (b) 10 μM aqueous fluorescein on a silver island film with 473 nm LED excitation and a 0.5 millivolt applied bias.

https://dx.doi.org/10.1021/acs.jpcc.9b11276
J. Phys. Chem. C 2020, 124, 5780−5788

voltage, increasing the temperature of the metal film also helps to increase electron transport between the discreet metal nanoparticles, which ultimately leads to an increased fluorophore-induced current signal. In addition, we have utilized the ratio of charging energy to thermal energy in order to characterize the ability for electron transport in our metal nanoparticle films, where the charging energy is determined with the concentric sphere model for capacitance of a metal nanoparticle. Finally, Figures 9 and 11show data collected with a low-power and low-cost LED excitation source. Given that our plasmonic current technique uses no traditional photodetector to detect the fluorescence and low-power excitation source, then we see promise for this technique in immunodiagnostic assays.

MATERIALS AND METHODS

Materials. Silver and gold pellets (99.999%) were purchased from Research and PVD Materials Corporation and Kurt J. Lesker, respectively. Various solvents used were purchased from Fisher Scientific. Fluorophores purchased from Sigma Aldrich include the following: fluorescein isothiocyanate (FITC), fluorescein sodium salt, rhodamine B, and sulforhodamine 101.

Metal Island Film Preparation: Thermal Vapor Deposition. Silane-prep glass microscope slides (Sigma-Aldrich) were first cleaned with methanol, dried under dry N_2, and subsequently used as a substrate for silver and gold vapor deposition. Metal films were prepared with an Edwards BOC Auto 306 Vapor Deposition Unit at a pressure of 9×10^{-6} torr. The deposition rate was held constant at 0.1 Å/s with deposition times ranging from 10 to 38 min. Prepared films were allowed to cool to room temperature and stored in a desiccator under vacuum until use.

Instrumentation. Absorption spectra of prepared silver and gold films were collected using a single beam Varian Cary 50-Bio UV−Vis spectrophotometer. Electrical current through the system was measured with a Keithley 6487 picoammeter/voltage source in either an open-circuit configuration or under an applied potential, with digital output to an external computer. Electrode materials were selected to match the metal nanoparticle film (for example, silver-on-silver). The electrodes were positioned to make simultaneous contact with the metal nanoparticle film and the liquid solvent. Scanning electron microscopy (SEM) of vapor-deposited films was performed using a Nova NanoSEM 450 with secondary electron imaging. A temperature-controlled stage was constructed using a Fisher Scientific IsoTemp Control Unit, and the temperature was monitored with a Fisher Scientific Traceable Infrared Non-Contact Laser Thermometer.

Fluorophore-Induced Current Measurements. Fluorophore solutions were prepared in various solvents, pipetted onto electrically non-continuous metal island films, and allowed to diffuse into the gaps between separate nanoparticle islands. Upon addition of solution to the metal, electrical current due to convection was allowed to stabilize for approximately 5 min. Fluorophores were chosen in order to provide optimal overlap between their emission and the metal nanoparticle film absorbance. Fluorophores were then excited with either a p-polarized LaserMate 473 nm continuous wave laser with the excitation power adjusted using an absorbing neutral-density filter wheel (Edmund Optics) or LED (various wavelengths with ∼1 mW irradiation intensity and ∼1 cm irradiation area) directed at the film surface. Change in electrical current through the fluorophore−metal system was monitored in an open-circuit configuration or under an applied potential over a range of temperatures and reported as the absolute value of current change, ΔI, with application of the excitation source. Unless indicated otherwise, measurements were conducted at room temperature (20 °C).

ASSOCIATED CONTENT

Supporting Information

The Supporting Information is available free of charge at https://pubs.acs.org/doi/10.1021/acs.jpcc.9b11276.

A table with size information for silver nanoparticle films (Table S1), scanning electron microscopy (SEM) images and corresponding particle size analyses (Figure S1), and absorption spectra of gold island films and corresponding fluorophore-induced current changes (Figure S2) (PDF)

AUTHOR INFORMATION

Corresponding Author

Chris D. Geddes − *Institute of Fluorescence and Department of Chemistry and Biochemistry, University of Maryland Baltimore County, Baltimore, Maryland 21202, United States*; Email: Geddes@umbc.edu

Authors

Joshua Moskowitz − *Institute of Fluorescence and Department of Chemistry and Biochemistry, University of Maryland Baltimore County, Baltimore, Maryland 21202, United States*; orcid.org/0000-0002-4768-9082

Rashad Sindi − *Institute of Fluorescence and Department of Chemistry and Biochemistry, University of Maryland Baltimore County, Baltimore, Maryland 21202, United States*

Complete contact information is available at: https://pubs.acs.org/10.1021/acs.jpcc.9b11276

Notes

The authors declare no competing financial interest.

ACKNOWLEDGMENTS

The authors would like to thank the Institute of Fluorescence along with the Department of Chemistry and Biochemistry at the University of Maryland Baltimore County (UMBC) for financial support. Also, special thanks to the UMBC Nanoimaging Facility for imaging used in this work.

ACRONYMS AND SYMBOLS

MEF	metal-enhanced fluorescence
$I_{fluorophore}$	induced electrical current from a fluorophore
I_{blank}	background current from a solvent
ΔI	electrical current change with application of an excitation source
ε	relative permittivity of the medium surrounding the metal particle
ε_0	vacuum permittivity
d	diameter of a spherical metal particle
r_0	radius of a spherical metal particle
s	distance between two spherical metal particles

https://dx.doi.org/10.1021/acs.jpcc.9b11276
J. Phys. Chem. C 2020, 124, 5780−5788

REFERENCES

(1) Mubeen, S.; Lee, J.; Lee, W.-r.; Singh, N.; Stucky, G. D.; Moskovits, M. On the Plasmonic Photovoltaic. *ACS Nano* **2014**, *8*, 6066−6073.

(2) Atwater, H. A.; Polman, A. Plasmonics for Improved Photovoltaic Devices. *Nat. Mater.* **2010**, *9*, 205−213.

(3) Tang, L.; Kocabas, S. E.; Latif, S.; Okyay, A. K.; Ly-Gagnon, D.-S.; Saraswat, K. C.; Miller, D. A. B. Nanometre-Scale Germanium Photodetector Enhanced By A Near-Infrared Dipole Antenna. *Nat. Photonics* **2008**, *2*, 226−229.

(4) Falk, A. L.; Koppens, F. H. L.; Yu, C. L.; Kibum, K.; de Leon Snapp, N.; Akimov, A. V.; Jo, M.-H.; Lukin, M. D.; Hongkun, P. Near-Field Electrical Detection of Optical Plasmons and Single-Plasmon Sources. *Nat. Phys.* **2009**, *5*, 475−479.

(5) Pelton, M.; Bryant, G. W. *Introduction to metal-nanoparticle plasmonics*; Wiley: Hoboken, New Jersey, 2013.

(6) Lakowicz, J. R. *Principles of Fluorescence Spectroscopy*; 3rd Ed.; Springer: New York, 2006.

(7) Gupta, R.; Dyer, M. J.; Weimer, W. A. Preparation and Characterization of Surface Plasmon Resonance Tunable Gold And Silver Films. *J. Appl. Phys.* **2002**, *92*, 5264−5271.

(8) Homola, J.; Piliarik, M. *Surface Plasmon Resonance Based Sensors*: Springer Series on Chemical Sensors and Biosensors; Springer: Berlin, 2006.

(9) Skoog, D. A.; West, D. M. *Principles of instrumental analysis*; Holt, Rinehart and Winston: New York, 2010.

(10) Wei, W.; Zhang, X.; Ren, X. Plasmonic Circular Resonators for Refractive Index Sensors and Filters. *Nanoscale Res. Lett.* **2015**, *10*, 211−211.

(11) Moskowitz, J.; Geddes, C. D. Plasmonic Electricity: Fluorophore-Induced Plasmonic Current. *J. Phys. Chem. C* **2019**, *123*, 27770−27777.

(12) Lakowicz, J. R. Radiative Decay Engineering 3. Surface Plasmon-Coupled Directional Emission. *Anal. Biochem.* **2004**, *324*, 153−169.

(13) Schmid, G. *Nanoparticles : From Theory to Application*; Wiley-VC: Weinheim, 2004.

(14) Kano, S.; Tanaka, D.; Sakamoto, M.; Teranishi, T.; Majima, Y. Control of Charging Energy In Chemically Assembled Nanoparticle Single-Electron Transistors. *Nanotechnology* **2015**, *26*, 045702−045702.

(15) Weaver, M. J.; Gao, X. Molecular Capacitance: Sequential Electron-Transfer Energetics For Solution-Phase Metallic Clusters In Relation To Gas-Phase Clusters And Analogous Interfaces. *J. Phys. Chem.* **1993**, *97*, 332−332.

(16) Garcia-Morales, V.; Mafé, S. Monolayer-Protected Metallic Nanoparticles: Limitations of The Concentric Sphere Capacitor Model. *J. Phys. Chem. C* **2007**, *111*, 7242−7250.

(17) Li, D.; Li, J. Preparation, Characterization And Quantized Capacitance Of 3-Mercapto-1,2-Propanediol Monolayer Protected Gold Nanoparticles. *Chem. Phys. Lett.* **2003**, *372*, 668−673.

(18) Wolfe, R. L.; Murray, R. W. Analytical Evidence For The Monolayer-Protected Cluster Au225[(S(CH2)5CH3)]75. *Anal. Chem.* **2006**, *78*, 1167−1173.

(19) Moore, R. G. C.; Evans, S. D.; Shen, T.; Hodson, C. E. C. Room-Temperature Single-Electron Tunnelling In Surfactant Stabilised Iron Oxide Nanoparticles. *Phys. E* **2001**, *9*, 253−261.

(20) Markovich, G.; Collier, C. P.; Heath, J. R. Reversible Metal-Insulator Transition In Ordered Metal Nanocrystal Monolayers Observed By Impedance Spectroscopy. *Phys. Rev. Lett.* **1998**, *80*, 3807−3810.

(21) Putnam, D. F. *Composition and Concentrative Properties of Human Urine*; Mcdonnell Douglas Astronautics Company. National Aeronautics and Space Administration, 1971, https://ntrs.nasa.gov/archive/nasa/casi.ntrs.nasa.gov/19710023044.pdf.

(22) Atkins, P. W.; De Paula, J., Keeler, J. *Atkins' Physical chemistry*; New Delhi: Oxford University Press, 2006.

(23) Hill, R. M. Electrical Conduction in Ultra Thin Metal Films. I. Theoretical. *Proc. R. Soc. London, Ser. A* **1969**, *309*, 377−395.

https://dx.doi.org/10.1021/acs.jpcc.9b11276
J. Phys. Chem. C 2020, 124, 5780−5788